Free-Space Laser Communication and Active Laser Illumination III, edited by David Voelz, Jennifer C. Ricklin, Proceedings of SPIE Vol. 5160, San Diego, CA, August 4 - 6, 2003.

Multi-loop control of a nanopositioning mechanism for ultra-precision beam steering

Jason J. Gorman*[a], Nicholas G. Dagalakis[a], Bradley G. Boone[b]

[a]Intelligent Systems Division, National Institute of Standards and Technology
100 Bureau Drive Stop 8230, Gaithersburg, MD 20899-8230

[b]Johns Hopkins University Applied Physics Laboratory
Johns Hopkins Road, Laurel, MD 20723-6099

ABSTRACT

Beam steering accuracy is critical to the successful operation of optical communications systems, especially those which take place over extreme distances, such as for an interstellar spacecraft. In this paper, a novel beam steering mechanism and several control system approaches for ultra-precision beam steering are discussed. The beam steering mechanism is a nanopositioning device which utilizes a parallel cantilever configuration and a piezoelectric actuator to obtain extremely high positioning accuracy with minimal parasitic errors. A robust motion controller is presented for this mechanism which is designed to compensate for modeling uncertainty. This controller is intended for use with feedback from the nanopositioner's built-in capacitance probe. Due to the need to track the trajectory of the steered beam, two additional control approaches are presented which combine the robust motion controller with additional feedback for the actual beam displacement. These multi-loop control approaches provide a level of robustness to thermal effects and vibrations which could not be obtained from a single sensor and feedback loop. Simulation results are provided for each of the control designs.

Keywords: beam steering, nanopositioner, multi-loop control, beam jitter, optical communication

1. INTRODUCTION

The development of optical communications capabilities between an interstellar explorer and a terrestrial target is a critical task for the success of future space missions. Boone et al.[1] have outlined a conceptual design for developing such a system. One particularly important feature in an optical communications system is the beam steering mechanism and its associated control system. Due to the extreme length over which the communication takes place, small perturbations of the beam azimuth and elevation angles, on the order of nanoradians, could cause faults in the communications link. In most existing space applications of optical communication, these perturbations can be controlled by closing the loop between the transmitter and receiver, such that the link remains locked. However, for long distance transmissions, this is not possible due to transmission latency. This requires the compensation of the perturbations locally, resulting in the need for ultra-precision pointing. In this paper, a novel beam steering mechanism and several control approaches are proposed for achieving the required level of pointing precision.

As discussed by Lambert and Casey[10], there are many different mechanisms for beam steering, all with different advantages and disadvantages. The most prevalent is the fast steering mirror which has proven to be effective in many functional optical communication systems. In an effort to achieve greater bandwidth, higher accuracy, and lighter and more compact mechanisms, other beam steering approaches have also been considered. Nikulin et al.[12] have studied the control of piezo-driven tip-tilt mirrors, among others. The modeling of acousto-optic deflectors (AOD) has been studied by Nikulin et al.[11] and Bouzoubaa et al.[2] have worked on the adaptive control of AODs. Optical phased arrays have also been investigated for use in high-precision beam steering by Ducharme et al.[4]. All of these approaches show promise in future optical communications systems. However, the research in this paper is concentrated on developing a beam steering mechanism which meets the specific criteria for the optical communications design presented by Boone et al.[1]. In their design, the optical train is configured such that all of the optics are located along a single axis. Furthermore, they

*Contact: gorman@cme.nist.gov

have put demanding constraints on the size, mass, and required power of the beam steering mechanism. Existing technology does not meet all of these requirements. Most importantly, fast steering mirrors increase the complexity of the optical train, and devices such as acousto-optical deflectors and optical phased arrays have a negative effect on the beam quality. Therefore, a new approach to beam steering has been adopted in this research.

The developed beam steering mechanism uses a nanopositioner to scan a lens in a plane while a beam is passed through the lens orthogonal to the motion plane. By scanning the lens, all of the optics can reside on a single axis and the quality of the beam is not adversely affected. In addition, this approach has several important advantages over other beam steering mechanisms. The nanopositioner has been shown to have extremely small off-axis parasitic errors. Also, the mechanism design is suitable for scale reduction, such that meso and micro scale devices could be developed in future design stages, resulting in a compact and lightweight solution. Section 2 presents the nanopositioner design and its application to beam steering. The modeling of this mechanism is presented in Section 3. The remaining sections of the paper are dedicated to control system approaches for the mechanism with application towards ultra-precision beam steering. First, a robust motion controller is discussed in Section 4, which is designed to compensate for modeling uncertainty, such as in the hysteresis of the nanopositioner piezoelectric actuator. The robust motion controller is then built upon to develop control architectures for ultra-precision beam steering. The robust motion controller is designed to use feedback from a capacitance probe. However, this does not provide feedback on the actual displacement of the beam. Therefore, two new control approaches have been developed, which are discussed in Section 5. These approaches combine feedback from the capacitance probe and an optical sensor to provide added robustness to thermal and vibration effects within the structure of the optical communication system. The results of simulation tests for each of these controllers are presented and discussed in Section 6, followed by conclusions and future extensions of this research.

2. BEAM STEERING USING A NANOPOSITIONER

A nanopositioning mechanism, or nanopositioner, is a device which has displacement resolution on the order of a few nanometers. Typically, these devices are constructed by integrating a flexure hinge mechanism with a piezoelectric actuator. The flexure hinge mechanism is a monolithic structure designed to deterministically deform under loading. The motion of the piezoelectric actuator is transmitted linearly through the flexure hinge mechanism, without any friction effects, resulting in high accuracy motion. In this paper, a single degree of freedom nanopositioner will be discussed, which is shown in Fig. 1. The flexure hinge mechanism utilizes a parallel cantilever design which results in very low cross-talk between the motion axes. The lever arms can also be used to amplify or attenuate the motion of the piezoelectric actuator depending on the application. Furthermore, the use of the four levers can effectively filter out off-axis parasitic motion in the actuator. A more rigorous discussion on these benefits has been presented by Dagalakis et al.[3]. In order to apply this design to beam steering applications, the mechanism has been scaled down in size by a factor of four. The piezoelectric actuator is connected to the flexure hinge mechanism using a coupler which uses a spherical flexure to minimize the moment placed on the actuator. This actuator has a range of 0 μm to 9.1 μm for an applied voltage range of 0 V to 150 V, resulting in a displacement range of 0 μm to 91 μm for the nanopositioner due to the motion amplification gain of ten in the flexure mechanism. The actuator and an attached lens can be seen in Fig. 1a. The flexures are not visible in the photograph due to their small thickness (100 μm). Therefore, a schematic is shown in Fig. 1b which indicates the location of each of the ten flexures.

A simple schematic describing the application of this nanopositioner to beam steering is shown in Fig. 2. The nanopositioner is drawn in cross-section, showing the location of a capacitance probe which measures the displacement of the mechanism. An aspheric lens is attached to the center of the nanopositioner. The laser source, which is assumed to be transmitted through a fiber optic cable, is positioned at a distance from the lens equal to the lens focal length, resulting in a collimated beam exiting the lens. Therefore, as the nanopositioner moves in the x direction, the beam angle θ changes such that $\theta \approx x/f$ where f is the focal length of the lens. Also included in this schematic is a quad photocell which measures the displacement of the exiting beam. The displacement of the beam in the optical sensor is defined as x_b and the beam path length from the lens to the optical sensor is defined as l. Therefore, the beam angle can also be defined as $\theta \approx x_b/l$. This results in the relation between the position of the nanopositioner and the beam displacement, such that $x = (f/l)x_b$. However, geometric uncertainties within the optical train can cause inaccuracies in this relationship. The control system designs discussed later in the paper will address the use of both the capacitance probe and quad photocell to achieve a robust beam steering system.

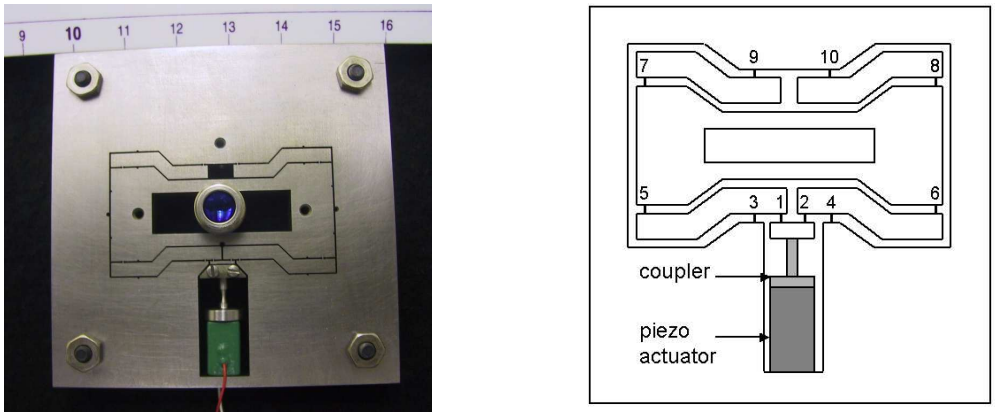

(a) (b)

Fig. 1 Beam steering nanopositioner (a) photograph of prototype (b) schematic showing flexures

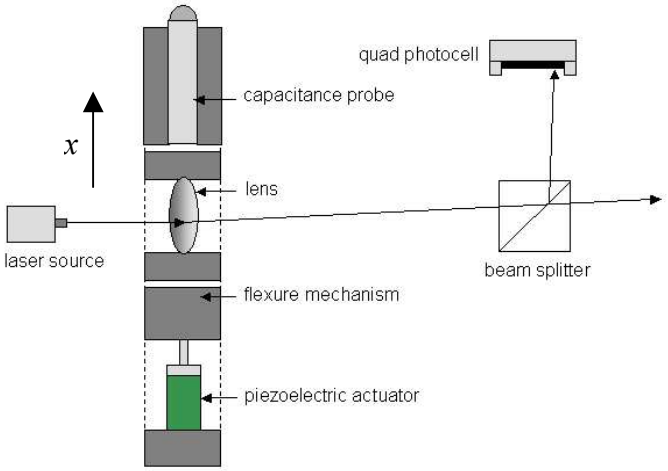

Fig. 2 Beam steering nanopositioner with capacitance probe and quad photocell feedback

Using this scanned lens approach presents several advantages beyond the resolution and accuracy provided by the nanopositioner. First, this configuration is insensitive to rotational errors about the beam axis. This is important because steered mirrors can have significant off-axis errors and alignment issues resulting in beam steering inaccuracies[9]. Second, unlike mirrors, the lens will not retain a large amount of heat transferred from the beam. This will minimize thermal expansion considerations and higher power lasers can be used, which may be needed for interstellar explorer missions. Finally, this configuration can be adapted to develop meso or micro scale beam steering elements. Due to the planar design of the nanopositioner, the mechanism could be micromachined using standard MEMS processes. This would enable the use of an array of high-precision beam steering elements, either in parallel or independently. An alternate approach to the presented design which is worth noting uses a stationary lens and attaches the fiber optic cable to the nanopositioner. Scanning the fiber optic cable instead of the lens will result in the same beam steering principle. However, due to the low mass and size of the cable, the nanopositioner can be redesigned to have higher bandwidth and be more compact. The modeling of this nanopositioner will be discussed in the following section.

3. NANOPOSITIONER MODELING

In this section, a dynamic model of the nanopositioner will be presented along with experimental results which have been used to verify and improve this model. A complete analytical model has already been discussed in Reference 8. Therefore, these results are only reviewed briefly. The model has been derived by considering the flexure mechanism and piezoelectric actuator separately, and then combining these results. The piezoelectric actuator and actuator coupler

have been modeled as discrete massless springs due to their low mass and high stiffness. The flexure mechanism is modeled as a second order system. The result is the following equation of motion:

$$M\ddot{x} + B\dot{x} + Kx = \frac{a}{b}\frac{k_c T}{k_a + k_c}\left(v_{in} - v_{rc}\right) \tag{1}$$

where M is the effective mass, B is the effective viscous damping coefficient, K is the effective stiffness coefficient, k_c is the stiffness of the actuator coupler, k_a is the stiffness of the piezoelectric actuator, T is the transformer ratio of the actuator, and b/a is the motion amplification gain. The inputs to the system are v_{in}, which is the voltage applied to the actuator, and v_{rc}, an internal voltage which causes hysteresis in the actuator motion. A complete description of the mass, M, and stiffness, K, parameters is given by Gorman et al.[8]. However, in the present development, only a model of the stiffness is necessary, which can be written as:

$$K = k_m + \frac{a^2}{b^2}\frac{k_a k_c}{k_a + k_c} \tag{2}$$

where k_m is the effective stiffness of the flexure mechanism. The nonlinear function describing the internal voltage v_{rc} is difficult to define. Goldfarb and Celanovic[7] have presented an approximate model for the electrical dynamics of a piezoelectric actuator which has been shown to predict the hysteresis accurately. However, in this paper, the hysteresis model will not be explored and the internal voltage, v_{rc}, will be treated as a bounded disturbance.

The left side of Eq. (1) represents a linear second order system. Therefore, the parameters M and B can be determined based on values for k_m, k_a, k_c, a/b, and the system natural frequency, ω_n and damping ratio, ξ. These parameters have been determined through experiments with the nanopositioner. First, static stiffness tests were performed to determine k_m and a/b. This was achieved by applying calibrated mass loads to the flexure mechanism and measuring the displacement. In the first test, shown in Fig. 3a, the load was applied to the actuator input. In the second test, shown in Fig. 3b, the load was applied directly to the output stage. These tests yielded a stiffness of k_m = 25148 N/m, and by comparing the two tests, it was found that a/b = 0.098. The natural frequency and damping ratio of the mechanism have been determined by experimentally measuring the frequency response. The results from this test are shown in Fig. 4. It is clear that the response is typical of a second order system, confirming the model presented in Eq. (1). Based on these results, it has been determined that ω_n = 1822 rad/s and ξ = 0.045. The stiffness of the actuator and coupler have been calculated using the published data from the actuator manufacturer, and the simple relation for a spherical flexure hinge (see Smith[13]), respectively, such that k_a = 1.859 x 10^8 N/m and k_c = 2.440 x 10^7 N/m. Based on these experiments and calculations, the effective mass and damping coefficient were found to be M = 0.07 kg and B = 11.47 N-s/m, which are reasonable for the mechanism.

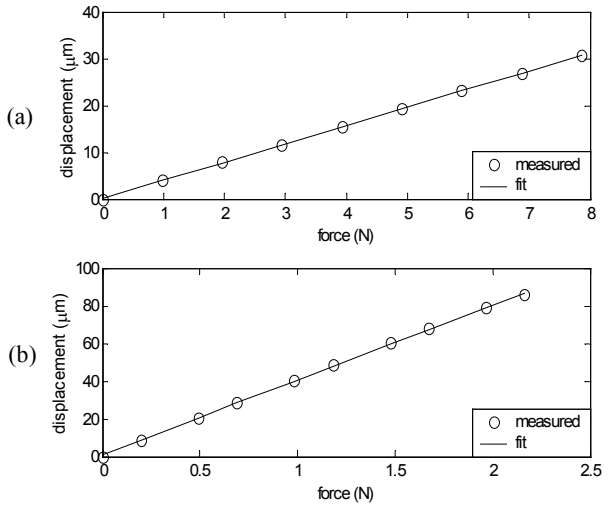

Fig. 3 Static stiffness test results for nanopositioner

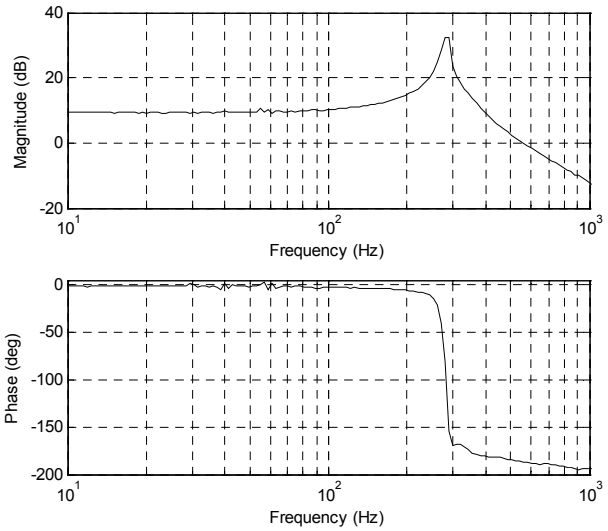

Fig. 4 Experimental frequency response function results

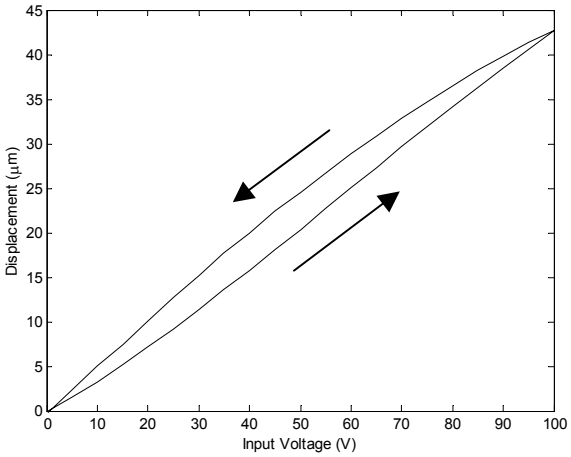

Fig. 5 Static input voltage vs. displacement results

In addition to these tests, the static behavior of the nanopositioner was examined to determine the transformer ratio T, and to find a bound on the internal voltage, v_{rc}, which causes the hysteresis in motion. The voltage applied to the actuator was increased and decreased from 0 V to 100 V several times, while the displacement was measured. The average voltage-displacement curve is shown in Fig. 5, which represents the major hysteresis loop for the voltage range of interest. The transformer ratio was calculated by using the slope of the increasing voltage curve, indicated by the arrow, resulting in a value of $T = 9.06$ C/m. A bound on the internal voltage v_{rc} can be found by noting the maximum difference in applied voltage between the rising and falling curves for the same displacement. This is found to be $v_{rc}^{*} = 9.5\,\mathrm{V}$, which will be used in the controller design. The presented model is quite simple, but closely fits the experimental frequency response function. This will now be used to design an appropriate controller for beam steering.

4. ROBUST MOTION CONTROL

A number of different approaches are available for controlling the second order dynamic model presented for the nanopositioner. However, due to the uncertainty in the internal voltage, v_{rc}, which causes hysteresis in the nanopositioner motion, a robust control approach which can compensate for this uncertainty is desirable. As previously discussed, the magnitude of the internal voltage can be bounded. Therefore, the sliding mode control theory has been selected for the design, which is a widely used approach to compensating for bounded uncertainty. In addition to the sliding mode controller, a full-state trajectory estimator is used to generate position, velocity and acceleration trajectories based on a reference position command. A second estimator is used to calculate estimates of the velocity of the nanopositioner. This combination of full state feedback and a full state trajectory is expected provide improved tracking performance compared to set point control, which is typically considered in beam steering control.

Applying sliding mode control to simple second order systems such as the nanopositioner dynamic model shown in Eq. (1) is fairly straightforward. Therefore, only an overview of the control design is provided here. Interested readers can look at the text by Edwards and Spurgeon[5] for further details. Before designing the controller, the model dynamics must be transformed into a set of error dynamics using the coordinate transformations $z_1 = x - x_d$ and $z_2 = \dot{x} - \dot{x}_d$, where x_d is the desired position trajectory. This results in the following error dynamics:

$$\dot{z}_1 = z_2 \tag{3}$$

$$\dot{z}_2 = -\frac{K}{M}x - \frac{B}{M}\dot{x} - \ddot{x}_d + \frac{a}{b}\frac{k_c T}{M\left(k_c + k_a\right)}\left(v_{in} - v_{rc}\right) \tag{4}$$

The first step in the sliding mode control design is to define a sliding surface, s, which renders the dynamic system in Eq. (3) stable when the system lies on the sliding surface, or when $s = 0$. In the case of second order systems, the sliding surface is typically chosen as a first order function such that:

$$s = z_2 + \lambda z_1 \tag{5}$$

where λ is a positive valued design parameter. Next, the sliding dynamics are derived by taking the time derivative of Eq. (5), which results in the following:

$$\dot{s} = -\frac{K}{M}x - \frac{B}{M}\dot{x} - \ddot{x}_d + \frac{a}{b}\frac{k_c T}{M\left(k_c + k_a\right)}\left(v_{in} - v_{rc}\right) + \lambda z_2 \tag{6}$$

The objective in designing the control law for the control input, v_{in}, is to make the sliding dynamics in Eq. (6) stable even though the internal voltage, v_{rc}, is an uncertain but bounded function. Therefore, the control law is chosen as:

$$v_{in} = -\frac{b}{a}\frac{M\left(k_c + k_a\right)}{k_c T}\left(-\frac{K}{M}x - \frac{B}{M}\dot{x} - \ddot{x}_d + \lambda z_2 + \phi s\right) - \frac{\rho s}{|s| + \varepsilon} \tag{7}$$

The parameters ϕ and ε are positive valued design constants and the switching gain ρ is chosen to counteract the uncertainty in v_{rc}. The last term in Eq. (7) is a continuous approximation to the discontinuous function used in sliding mode control. Substituting Eq. (7) into Eq. (6), and assuming that all system parameters are known exactly except for v_{rc} results in the following closed-loop sliding dynamics:

$$\dot{s} = -\phi s - \frac{a}{b}\frac{k_c T}{M\left(k_c + k_a\right)}\left(\frac{\rho s}{|s| + \varepsilon} + v_{rc}\right) \tag{8}$$

The switching gain ρ is chosen such that $\rho > v_{rc}$ to guarantee that the sliding dynamics are stable and ultimately bounded. Assuming that v_{rc} has an upper bound v_{rc}^*, which was discussed when presenting the model, then the switching gain is selected as $\rho = \eta v_{rc}^*$ where η is a positive valued constant such that $\eta > 1$. Since the continuous approximation is used instead of the discontinuous function for the sliding mode control, the tracking will not be guaranteed to go to zero. However, the tracking error is bounded based on the choice of η and ε. This bound on reaching the sliding surface can be determined using Lyapunov stability theory to be $|s| \le \varepsilon/(\eta - 1)$. The bound on the position tracking error is then found to be $|z_1| \le \varepsilon/(\lambda(\eta - 1))$. Therefore, the tracking error can be improved by increasing λ, increasing η, and decreasing ε. However, as the tracking error is improved by tuning these parameters, the controller approaches the form of a discontinuous function, which can cause chattering in the position and high frequency oscillations in the control input. The presented sliding mode control design could also be used to compensate for uncertainty in the model parameters such as the mass and stiffness, but this was omitted for simplicity.

Although this controller can be extremely effective in compensating for the uncertainty, there are two complications in implementing this controller. The first is that full state feedback is required. This is a problem since the capacitance probe and quad photocell will only provide position feedback. The second is that a full-state trajectory is required including the desired position, velocity and acceleration. Therefore, in order to implement this controller, the velocity of the nanopositioner and the desired trajectory must be estimated. The approach which will be used is a high-gain observer which has been discussed by Esfandiari and Khalil[6]. Since the approach for estimating the velocity and the trajectory is similar, only the high-gain observer for the desired trajectory will be presented here. The equations for this observer can be written as:

$$\begin{bmatrix} \dot{y}_1 \\ \dot{y}_2 \\ \dot{y}_3 \end{bmatrix} = \begin{bmatrix} -\beta_1/\tau & 1 & 0 \\ -\beta_2/\tau^2 & 0 & 1 \\ -\beta_3/\tau^3 & 0 & 0 \end{bmatrix} \begin{bmatrix} y_1 \\ y_2 \\ y_3 \end{bmatrix} + \begin{bmatrix} \beta_1/\tau \\ \beta_2/\tau^2 \\ \beta_3/\tau^3 \end{bmatrix} r \tag{9}$$

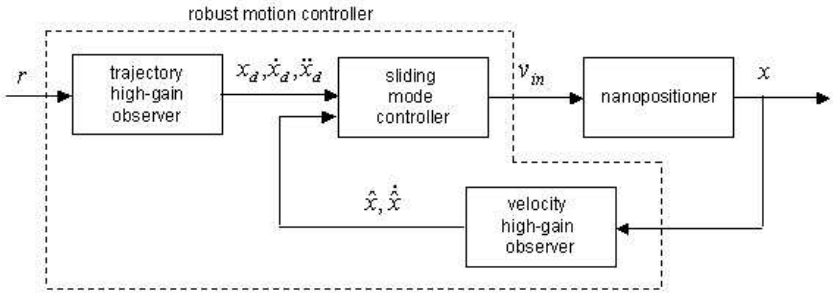

Fig. 6 Closed-loop system with robust motion controller

The input to the observer is the tracking reference signal, *r*, which provides the desired position. The output of the observer is the complete trajectory where $x_d = y_1$, $\dot{x}_d = y_2$, and $\ddot{x}_d = y_3$. The bandwidth of the observer is set by the choice of the gains β_1, β_2, and β_3. Furthermore, the accuracy of the estimation of the trajectory can then be tuned by adjusting the parameter τ. This estimator is called a high-gain observer because as τ approaches zero, the estimate becomes exact. However, the high gain and peaking which results when making τ very small presents a limit on the accuracy of the obtainable estimate. The observer for estimating the actual velocity of the nanopositioner will be similar to the observer shown in Eq. (9). However, the order of the observer will be two instead of three and the input to the observer will be the measured position. In both cases, a reduced order observer can also be used in which the order of the observer is reduced by one due to available position and desired position feedback.

The combination of the sliding mode controller and the two high-gain observers will serve as the robust motion controller for the nanopositioner. A block diagram of the closed loop system using these components is shown in Fig. 6. The robust controller has two inputs, the desired position reference signal, *r*, and the measured position, *x*, and outputs the voltage, v_{in}, to the actuator. This modular control design can then be used for a number of different purposes. In the following two sections, control architectures will be presented which use this component as the basis for more complex control systems which address external disturbances due to thermal and structural disturbances which can be sensed in the optical train.

5. MULTI-LOOP CONTROL APPROACHES

The robust motion controller has been designed to control the motion of the nanopositioner using position feedback from the capacitance probe. This collocated sensing and control approach guarantees that the nanopositioner is stable during operation. However, since the controller does not utilize sensing information for the actual beam angle, there is no guarantee that the beam will track the desired position. Since there will be a significant set of optics in the optical train after the beam passes through the nanopositioner, it is expected that there will be some uncertainty in the relationship between the motion of the beam and the motion of the nanopositioner. This uncertainty may be the result of thermal effects or vibrations in the supporting structure. Therefore, two approaches to incorporating the robust motion controller with sensing of the beam angle to compensate for this uncertainty are proposed in the following two subsections. Both of these controllers make use of an optical sensor, as discussed in previous sections, located near the end of the optical train to measure the deflection of the beam before the beam leaves the system. The first controller adds an additional control loop around the robust motion controller to compensate for uncertainty in the relationship between the position of the nanopositioner and the resulting beam angle. The second controller compensates for vibrations in the optical train which can be sensed by the optical sensor. In both cases, the improvements are introduced by modifying the tracking signal sent to the robust motion controller. These multi-loop approaches provide robustness to uncertainties which could not be addressed by the robust motion controller alone.

5.1 Dual-loop control for optical uncertainty compensation

Although the optical bench for an optical communication system is designed to minimize structural distortions due to thermal effects, uncertainties in the dimensions of the optical structure on the order of a few micrometers are inevitable. Changes in the dimensions of the optical structure result in a change in the relationship between the position of the nanopositioner and the beam angle. In this section, a controller is proposed which uses the optical sensor data along with the robust motion controller, to improve the beam steering accuracy when there is uncertainty in the optics geometry.

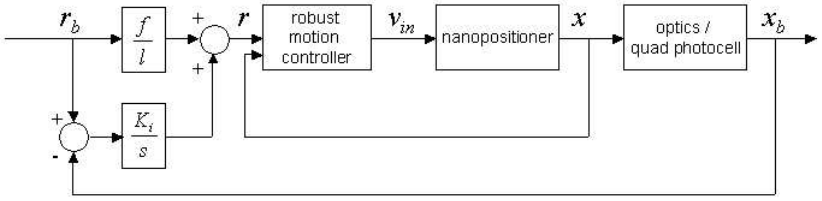

Fig. 7 Multi-loop control system with beam error integrator

The approach used to address this problem is a modification of dual-loop control, which is often used in motion control problems. When a motor is attached to a gear train, there tends to be some level of backlash in the system due to spacing between the gear teeth. This nonlinearity between the input of the motor and the output, which may be a gear or motion stage, can result in errors in the output tracking and can also make the system unstable. One solution is to measure both the motor motion and the output motion, and then design a controller using both sensors for feedback. In many cases, this approach can stabilize the motion and make the tracking error very small. In the case of the beam steering system, there are also two sources of feedback and an uncertain, possibly nonlinear, function relating this feedback. Therefore, the dual-loop approach has been found to be an attractive option for integrating the optical sensor feedback with the robust motion controller. However, the standard dual loop controller is not applicable directly, so the necessary modifications are discussed below.

The dual-loop approach designed for the beam steering system is shown in Fig. 7. The robust motion controller acts as the internal loop and a second feedback loop is built around this controller. The interface between the robust motion controller and the outer loop is through the modification of the position reference signal fed into the inner loop. The desired beam position on the optical sensor, r_b, is the reference signal to the system. This signal is scaled using the known, but uncertain, relationship between the beam position in the optical sensor, x_b, and the nanopositioner position, x, such that $x = (f/l)x_b$ where f is the focal length of the scanned lens and l is the length of the beam path between the lens and optical sensor. The position reference signal sent to the robust motion controller is then calculated as:

$$r = \frac{f}{l} r_b + K_i \int_0^t (r_b - x_b) d\xi \tag{10}$$

The first term in Eq. (10) is the standard tracking signal, which would be satisfactory if there was no uncertainty between x and x_b. The second term in Eq. (10) compensates for the expected uncertainty by using an integral control term for the position tracking error for the beam displacement. The integral gain K_i must be tuned for the desired performance. The proposed design differs from the standard dual-loop approach in that the outer loop is used to modify the position reference signal to the robust motion controller, instead of directly modifying the control input v_{in}. This is motivated by the fact that the sliding mode controller has been specifically designed to reject additive voltage signals into the nanopositioner. If the integral control term was fed directly into the nanopositioner, the sliding mode controller would compensate for this disturbance and the mechanism would continue to track the original reference signal. Therefore, the correction to the motion control must be applied through the position reference signal, which is tracked using the sliding mode controller. The drawback of this approach is that the bandwidth is limited by the inner loop. Simulation results for this approach will be presented and discussed in a later section.

5.2 Trajectory correction for vibration compensation

Another form of uncertainty which can enter into the optical train between the nanopositioner and the output of the beam is a disturbance due to structural vibrations, which causes pointing errors. It is assumed in this case that the vibrations affect only the portion of the optical train after the nanopositioner. Therefore, these vibrations can be sensed in the beam motion, but not in the position of the nanopositioner, such that they appear as an injected disturbance into the optics. An alternate problem, in which the base of the nanopositioner is vibrating during beam pointing, has also been considered by Gorman et al.[8]. This current problem can be addressed by generating a correction to the position reference signal, r, based on sensing the vibrations. The capacitance probe and optical sensor measurements are compared, and the difference between the two is assumed to be the motion due to vibrations in the optics. The reference signal can be modified based on this principle such that:

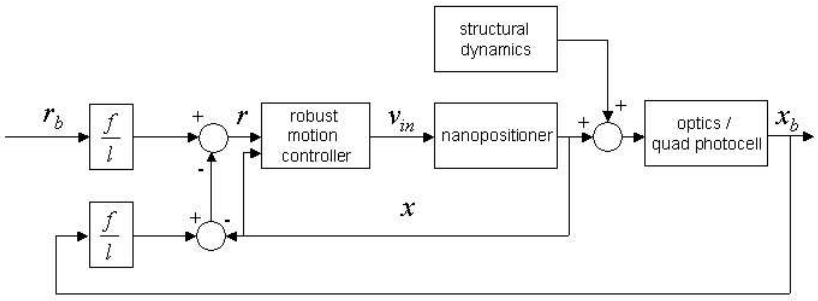

Fig. 8 Multi-loop control system with vibration compensation

$$r = \frac{f}{l} r_b - \left(\frac{f}{l} x_b - x \right) \tag{11}$$

This control approach is shown in Fig. 8. The outer loop is strictly algebraic, resulting in a simple correction of the trajectory which counteracts the motion due to vibrations. This approach is only valid if the vibrations are on the order of or smaller than the possible motion of the nanopositioner. However, it is a valid assumption that the optical train will utilize vibration isolation. Therefore, the amplitude of the vibrations are expected to be small, but large enough to have a significant effect on the beam steering accuracy. Furthermore, the degree to which the robust motion control loop can compensate for these vibrations is dependent on the combined achievable bandwidth of the mechanism and the controller. A much better approach to compensating for the vibrations is to apply active control within the optical train. However, in most cases this is unlikely, and the proposed approach will provide some level of rejection of the motion due to vibrations. Another important note is that this control approach is dependent on perfect knowledge of the geometry of the optics. Any uncertainty in this respect would make this problem significantly more difficult. Simulation results for this approach will be presented and discussed in the following section.

6. SIMULATION RESULTS

The three control systems discussed in Sections 4, 5.1 and 5.2, respectively, have been tested using numerical simulation. In these simulations, the model of the nanopositioner discussed in Section 3 was used including all of the listed system parameters. However, these simulations do not contain a model of the hysteresis of the piezoelectric actuator. In future work, the piezoelectric actuator will be characterized using the modeling approach of Goldfarb and Celanovic[7]. However, the simulations do provide some measure of how well the robust motion controller will work. Most importantly, they demonstrate the effectiveness of the multi-loop approaches compared to single loop controllers.

6.1 Robust motion control

There are a number of design parameters which must be chosen appropriately to achieve satisfactory results when using the robust motion control discussed in Section 4. However, these parameters can typically be tuned to achieve the desired response, although as the gain of the system increases there will be a noticeable increase in the control effort. In the simulation test presented in this section, the gains were selected to achieve reasonable bandwidth, which is on the order of 100 Hz. The important parameters for the sliding mode controller are $\eta = 2$, $\varepsilon = 0.1$, $\lambda = 2937$, and $\phi = 1210$, where λ and ϕ were designed such that the linearized closed-loop system has a natural frequency and damping ratio of $\omega_{nd} = 1885$ rad/s and $\xi_d = 1.1$. In addition, the gains for the high-gain observers were chosen to have similar bandwidth as the controller.

The controller was tested in simulation by providing a sinusoidal position reference input to the closed loop system and measuring the resulting position of the dynamic model. In all cases, the position reference signal was chosen to have an amplitude of 5 μm and have a bias of 20 μm. Fig. 9 shows the system response to a 20 Hz reference signal, including the position response, tracking error, and control effort. The steady state tracking error is less than 0.03 μm, which is only a 0.6 % error, when compared to the amplitude of the reference signal. The controller was tested over a range of

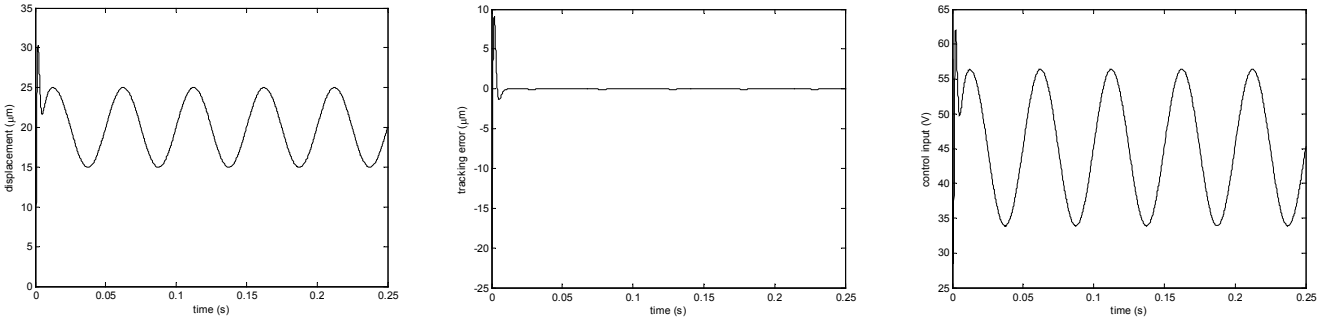

(a) (b) (c)

Fig. 9 Results for a 20 Hz reference signal (a) position (b) tracking error (c) control effort

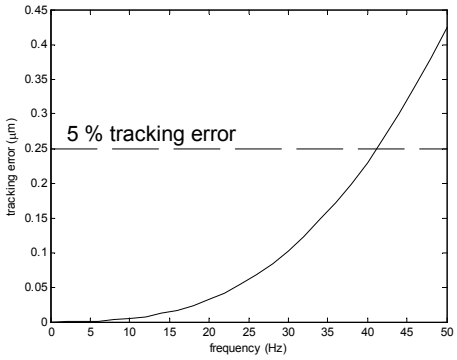

Fig. 10 Tracking frequency response

frequencies for the reference signal and the steady state error was measured. The results of this test are shown in Fig. 10, where the horizontal dotted line represents the cutoff for a tracking error below 5 %. This plot shows that the controller can maintain a tracking error below 5 % up until 40 Hz. The 5 % bound was chosen just as a reference since actual performance requirements are not known at this time. However, the tracking bandwidth could be extended if necessary by redesigning the gains. These results demonstrate the effectiveness of combining the sliding mode controller with the two high-gain observers.

6.2 Dual loop control for optical uncertainty compensation

The dual loop controller presented in Section 5.1 was tested in simulation using the same robust motion controller parameters discussed in the previous section. The objective of these simulations was to demonstrate that the added loop could be used to compensate for uncertainty in the optics geometry. The relationship between the position of the nanopositioner and the displacement of the beam is assumed to be described by the simple equation $x = (f/l)x_b$. As a demonstration of the robustness of this approach, the nominal value of the ratio f/l was chosen to be 0.1. However, the actual value of the ratio was set to be 0.18. The robust motion controller alone, and the dual loop controller were tested to see if a 1 Hz square wave could be tracked even with the optics geometry uncertainty. The results of this test are shown in Fig. 11. The robust motion controller has a significant offset and the square wave is of smaller amplitude than the desired signal, which is a result of the uncertainty. The dual loop controller, which used an integral gain $K_i = 10$, is able to track the square wave with very small errors. This performance was achieved with a limited amount of tuning effort. The transient response can be improved further by increasing K_i. However, if K_i is increased beyond the bandwidth of the robust motion controller, the system may become unstable. This test shows the effectiveness of the dual-loop approach to uncertainties in the linear relationship between the nanopositioner position and the beam displacement. However, further tests will be required to determine whether this approach can also compensate for nonlinear and time-varying uncertainties in the relationship.

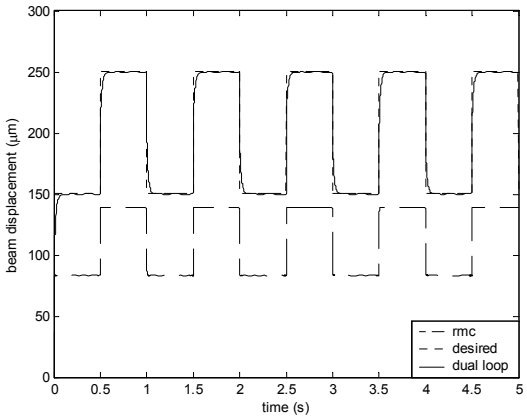

Fig. 11 Tracking control with uncertainty in the optics geometry

6.3 Trajectory correction for vibration compensation

In this final test, the vibration compensation approach was implemented. The vibrations present in the optical structure were assumed to be at 10 Hz and have a steady state amplitude of 30 μm. The objective of the test was to see how well the controller could track a 1 Hz sinusoidal trajectory with a beam displacement amplitude of 50 μm and a bias of 200 μm, while the optical structure is vibrating. Initially, only the robust motion controller was used which resulted in poor tracking results, as shown in Fig. 12a. However, when the outer control loop was used for trajectory correction, the controller showed significant improvement as shown in Fig. 12b. Although the tracking results are not perfect, it is clear that optical communications systems could benefit from this approach when active vibration control is not available in the optical structure.

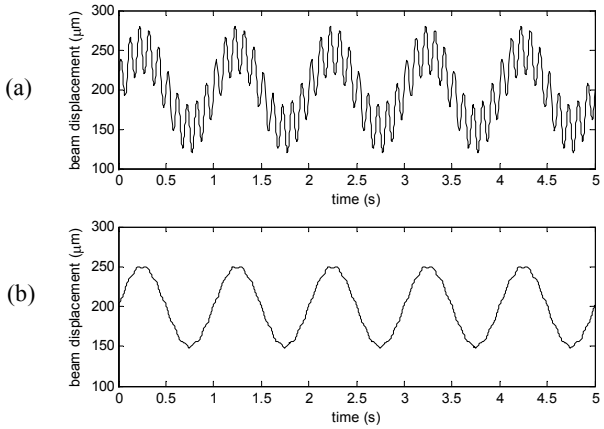

Fig. 12 Control of vibrations a) no compensation b) compensation using trajectory correction

7. CONCLUSION

This paper has provided a proposal for a novel beam steering mechanism and several control approaches which will enable ultra-precision beam steering for future space missions. The beam steering mechanism, which is a nanopositioner, has been modeled using a combination of analytical and experimental methods, resulting in a straightforward equation of motion. The control designs presented concentrated on providing robustness to modeling uncertainties and external disturbances. The first controller, which was the robust motion controller, utilizes collocated feedback to compensate for modeling uncertainty by using a combination of sliding mode control and two high-gain observers. The sliding mode controller is used to guarantee stability and performance bounds based on *a priori*

knowledge of the model uncertainty. The high-gain observers provide estimates for the desired trajectory based on a reference signal, and the nanopositioner velocity using the measured position. This controller component was then used to develop two multi-loop control designs which incorporate direct sensing of the beam displacement using an optical sensor. The first multi-loop controller uses the optical sensor feedback to provide robustness to uncertainty in the geometry of the optical train, which can be caused by thermal effects and structural distortions. The second multi-loop controller is designed to reject vibrations in the optical structure which can be sensed in the optical sensor.

All three of these controllers have been demonstrated in simulation and have been shown to effectively provide robust tracking. However, these results are only the initial tests for the proposed controllers. In future work, these algorithms will be implemented on the actual nanopositioner, using the capacitance probe and quad photocell for feedback. The robustness to the hysteresis in the piezoelectric actuator will then be investigated in more detail. In addition, the sensitivity of these control approaches to sensor noise will be evaluated.

ACKNOWLEDGEMENTS

This research was performed while the first author held a National Research Council Postdoctoral Research Associateship Award at the National Institute of Standards and Technology.

REFERENCES

1. B. G. Boone, R. S. Bokulic, G. B. Andrews, R. L. McNutt Jr., & N. Dagalakis, "Optical and microwave communications system conceptual design for a realistic interstellar explorer," *Proceedings of SPIE - Free-Space Laser Communication and Laser Imaging II*, SPIE Vol. 4821, Seattle, WA, pp. 225-236, 2002.
2. M. Bouzoubaa, V. V. Nikulin, V. A. Skormin, & T. E. Busch, "Model reference control of a laser beam steering system for laser communication applications," *Proceedings of SPIE – Free-Space Laser Communication Technologies XIII*, SPIE Vol. 4272, San Jose, CA, pp. 93-103, 2001
3. N. G. Dagalakis, J. A. Kramar, E. Amatucci, & R. Bunch, "Kinematic modeling and analysis of a planar micro-positioner," *Proceedings of the ASPE Annual Meeting*, Crystal City, VA, pp. 135-138, 2001.
4. A. D. Ducharme, G. Wyntjes, C. Markos, & G. D. Boreman, "Precision closed loop control of optical beam steering," *Proceedings of SPIE – Spatial Light Modulators*, SPIE Vol. 3292, San Jose, CA, pp. 129-138, 1998.
5. C. Edwards & S. K. Spurgeon, *Sliding Mode Control: Theory and Applications*, Taylor & Francis: London, 1998.
6. F. Esfandiari & H. K. Khalil, "Output feedback stabilization of fully linearizable systems," *International Journal of Control*, Vol. 56, pp. 1007-1037, 1992.
7. M. Goldfarb & N. Celanovic N., "Modeling piezoelectric stack actuators for control of micromanipulation," *IEEE Control Systems Magazine*, Vol. 17, pp. 69-79, 1997.
8. J. J. Gorman & N. G. Dagalakis, "Modeling and disturbance rejection control of a nanopositioner with application to beam steering," to appear in *Proceedings of the ASME IMECE*, Washington, DC, 2003.
9. R. E. Hopkins & D. Stephenson, "Optical systems for laser scanners," in *Optical Scanning*, ed. G. F. Marshall, Marcel Dekker: New York, 1991.
10. S. G. Lambert & W. L. Casey, *Laser Communications in Space*, Artech House: Boston, 1995,
11. V. V. Nikulin, M. Bouzoubaa, V. A. Skormin, & T. E. Busch, "Modeling of an acousto-optic laser beam steering system intended for satellite communication," *Optical Engineering*, Vol. 40, pp. 2208-2214, 2001.
12. V. V. Nikulin, M. Bouzoubaa, V. A. Skormin, & T. E. Busch, "Decentralized adaptive control for laser beam tracking systems," *Proceedings of SPIE – Free-Space Laser Communication Technologies XIII*, SPIE Vol. 4272, San Jose, CA, pp. 200-208, 2001.
13. S. T. Smith, *Flexures: Elements of Elastic Mechanisms*, Gordon & Breach: Amsterdam, 2000.